frontiers in Water

ORIGINAL RESEARCH
published: 21 March 2022
doi: 10.3389/frwa.2022.827923

Predicting the Rate Coefficients of Attachment and Detachment of Colloids in Saturated Porous Media

*Yerramilli Sai Rama Krishna and N. Seetha**

Department of Civil Engineering, Indian Institute of Technology Hyderabad, Sangareddy, India

The transport behavior of pathogenic microorganisms and nanoparticles (NPs) in the subsurface is usually studied by performing laboratory soil column experiments. Parameters describing colloid deposition on grain surfaces are estimated by fitting observed breakthrough curves with an appropriate one-dimensional model. However, predictive tools to estimate colloid deposition parameters, knowing the system properties such as soil type, colloid type, solution chemistry, and flow velocity, are useful in estimating the travel distances of pathogenic microorganisms in the subsurface. Such predictive models are rare, except the colloid attachment rate coefficient predicted by colloid filtration theory (CFT) under favorable conditions. Although a couple of theoretical and empirical predictive models are available for estimating the deposition parameters under unfavorable conditions, they were developed for a small set of data, and their applicability to a wide range of conditions is unexplored. In this study, several sets of column-experimental data from literature, covering a wide range of experimental conditions, were analyzed to understand key factors that control colloid deposition. Empirical relationships were developed for deposition rate coefficients and sticking efficiency of various colloidal types [viruses, bacteria, graphene oxide (GO) NPs, silver (Ag) NPs, titanium dioxide (TiO_2) NPs, and carboxylate-modified latex (CML) colloids] vis-à-vis 11 physicochemical parameters such as porosity, mean pore-water velocity, median grain size, colloid radius, solution ionic strength, surface potentials of colloids and grains, Hamaker constant, temperature, viscosity of water, and dielectric constant. While deposition of viruses and CML colloids on grain surfaces was found to be reversible, deposition of bacteria, GO NPs, Ag NPs, and TiO_2 NPs was found to be irreversible. The empirical equations proposed in this study can predict deposition rate coefficients more closely ($p < .001$, $R^2 = 0.69 - 0.85$) than CFT ($p < .7$, $R^2 \leq 0.41$). The performance of CFT in predicting the attachment rate coefficients of viruses, bacteria, GO NPs, TiO_2 NPs, and CML colloids was found to improve significantly when estimated rate coefficients were multiplied by the sticking efficiency calculated using the empirical expression proposed in this study ($p < .001$, $R^2 = 0.65 - 0.95$).

Keywords: colloids, viruses, bacteria, nanoparticles, deposition, attachment rate coefficient, porous media

OPEN ACCESS

Edited by:
Jan Willem Foppen, IHE Delft Institute for Water Education, Netherlands

Reviewed by:
Vasileios Katzourakis, Technical University of Crete, Greece
Vasiliki Syngouna, University of Patras, Greece

****Correspondence:***
N. Seetha
seetha@ce.iith.ac.in

Specialty section:
This article was submitted to Environmental Water Quality, a section of the journal Frontiers in Water

Received: *02 December 2021*
Accepted: *07 February 2022*
Published: *21 March 2022*

Citation:
Krishna YSR and Seetha N (2022) Predicting the Rate Coefficients of Attachment and Detachment of Colloids in Saturated Porous Media. Front. Water 4:827923. doi: 10.3389/frwa.2022.827923

INTRODUCTION

Colloidal contaminants, such as pathogenic microorganisms (viruses, bacteria, and protozoa) and engineered nanoparticles (ENPs) enter the subsurface from various sources, including landfill leachates, industrial discharges, and land application of wastewater. Understanding the fate and transport of colloids in the subsurface is therefore essential to prevent groundwater contamination and protect human health.

The various mechanisms for retention of colloids in soil include deposition on grain surfaces, blocking, straining, and ripening. Colloid transport in porous media is usually studied by performing soil column experiments in the laboratory, and colloid retention parameters (attachment and detachment rate coefficients, maximum adsorption capacity of the soil, and straining coefficient) are in turn estimated by fitting the observed breakthrough curves with one-dimensional advection-dispersion equation with terms accounting for appropriate retention mechanisms. Literature shows that the rate coefficients of attachment and detachment of colloids to grain surfaces depend on various physicochemical factors, such as, flow velocity (Hendry et al., 1999; Tong and Johnson, 2006; Syngouna and Chrysikopoulos, 2013; Sasidharan et al., 2017a), grain size (Bradford et al., 2003; Knappett et al., 2008; Mitropoulou et al., 2013; Bai et al., 2016), colloid size (Tong and Johnson, 2006; Johnson et al., 2007), solution pH (Jewett et al., 1995; Sadeghi et al., 2011; Fang et al., 2013), ionic strength (Li et al., 2004; Johnson et al., 2007; Torkzaban et al., 2008a; Sadeghi et al., 2011; Fang et al., 2013), soil type (Chu et al., 2003; Schinner et al., 2010), colloid type (Li et al., 2004; Li and Johnson, 2005; Bai et al., 2016; Hedayati et al., 2016; Sasidharan et al., 2017a), temperature (Kim and Walker, 2009; Chrysikopoulos and Aravantinou, 2014; Schijven et al., 2016; Sasidharan et al., 2017b), and type of soil treatment (Tian et al., 2010). Predictive tools to estimate colloid attachment and detachment rate coefficients as functions of various physicochemical parameters influencing them will be useful in estimating the travel distances of various colloidal contaminants in groundwater (Schijven et al., 2000). However, such tools are rare, except for the theoretical expression for attachment rate coefficient under favorable conditions (interaction energy between colloid and grain surface being attractive at all separation distances) given by the colloid filtration theory (CFT; Yao et al., 1971), which describes deposition using a first-order irreversible kinetic model. However, environmental conditions in the subsurface are predominantly unfavorable for deposition (Ryan and Elimelech, 1996; Wan and Tokunaga, 2002). Unfavorable conditions for deposition arise when the interaction energy profile between the colloid and grain surface contains an energy barrier (Tufenkji and Elimelech, 2005). Under unfavorable conditions, colloid detachment from the grain surface is also important, and hence, deposition is usually described using a reversible kinetic model. Since the rate of deposition under unfavorable conditions is lower than under favorable conditions, the expression for attachment rate coefficient given by CFT is multiplied by a factor, α ($\alpha < 1$), called the sticking efficiency. Sticking efficiency is affected by various factors, such as, flow velocity, grain size, colloid size, solution pH and ionic strength, soil type, colloid type, and temperature (Keller et al., 2004; Tong and Johnson, 2006; Shen et al., 2008). However, theoretical expressions to estimate the value of α as a function of the above-mentioned system parameters are not available. Bai and Tien (1999), Elimelech (1992), Park et al. (2012), and Sadeghi et al. (2011) derived empirical expressions for α in terms of the various factors affecting it. Bai and Tien (1999) used several sets of experimental data on the transport of polystyrene latex particles through columns packed with glass beads, and derived a correlation equation for α in terms of flow velocity, colloid size, solution ionic strength, surface potentials of colloid and collector, temperature, viscosity, Hamaker constant, and dielectric constant of water. Elimelech (1992) used a semi-empirical approach to derive a quantitative relationship between α and parameters characterizing the system chemistry (colloid size, surface potentials of colloid and collector, ionic strength, and Hamaker constant) for the transport of latex particles through glass bead–packed columns. Park et al. (2012) and Sadeghi et al. (2011), using several sets of experimental data on the transport of *Cryptosporidium parvum Oocysts* and bacteriophage PRD1 through columns packed with sand or glass beads, derived empirical equations for α as a function of pH and ionic strength. The above empirical expressions were derived considering only a subset of factors affecting α, and their applicability to a wider range of experimental conditions is unexplored.

Although colloid detachment from grain surfaces is important under unfavorable conditions, no quantitative relationship between the detachment rate coefficient and the factors affecting it exists, except for the correlation equation for nanometre-sized particles derived by Seetha et al. (2015a, 2017). Seetha et al. (2015a, 2017) upscaled nanoparticle (NP) transport in porous media under unfavorable conditions from pore to the Darcy scale using pore network modeling, and derived correlation equations for attachment and detachment rate coefficients in terms of 10 Darcy-scale parameters, including porosity, mean pore radius, mean pore-water velocity, NP radius, ionic strength, dielectric constant, surface potentials of colloid and collector, temperature, and viscosity of the solution. They also derived expressions for attachment efficiency as a function of the above parameters. However, since Seetha et al. (2015a, 2017) assumed that surface properties of the porous medium and NPs were homogeneous, and NPs were spherical in shape, they did not account for the effect of: (a) heterogeneity of the grain surface and NPs and (b) shape of the NPs on particle deposition.

Quantitative relationships between attachment and detachment rate coefficients of colloidal contaminants, such as viruses, bacteria, and ENPs, and the various physicochemical parameters controlling them have not been developed yet. Empirical expressions offer the advantage of accounting for additional factors influencing colloid deposition, such as heterogeneity of grain surfaces and colloids and the shape of colloids, which are difficult to account for in theoretical models. In this study, several sets of column-experimental data for a variety of experimental conditions reported in literature were analyzed, and empirical relationships between

attachment and detachment rate coefficients vis-à-vis the various physicochemical system parameters were developed for the transport of viruses, bacteria, graphene oxide (GO) NPs, silver (Ag) NPs, titanium dioxide (TiO_2) NPs, and carboxylate-modified latex (CML) colloids through porous media composed of glass beads or quartz sand.

METHODOLOGY

Experimental Data to Develop Empirical Equations

Literature shows that the rate coefficients for colloid (viruses, bacteria, ENPs, and CML colloids) attachment to, and detachment from grain surfaces depend on 11 physicochemical parameters (Seetha et al., 2017): porosity (θ [-]), mean pore-water velocity ($\overline{v}$ $\left[\frac{L}{T}\right]$), median grain size (d_{50} $[L]$), colloid radius (a $[L]$), solution ionic strength (I $[Molar]$), surface potentials of colloids ($\psi_c[ML^2T^{-3}I^{-1}]$) and grains ($\psi_g[ML^2T^{-3}I^{-1}]$), Hamaker constant (H $[ML^2T^{-2}]$), temperature (T $[K]$), viscosity of water (μ $[ML^{-1}T^{-1}]$), and dielectric constant (ε [-]). Hence, experimental data from research papers that reported all the above-listed parameter values, along with values of deposition rate coefficients for colloid transport through laboratory columns, were selected. In this study, only data from experiments performed using a monovalent background electrolyte were considered. There can be multiple retention mechanisms involved in the transport of colloids reported in a given study. For example, Qi et al. (2014) studied the transport of GO NPs through columns packed with quartz sand, and the transport behavior was described using a model that accounted for irreversible attachment and straining. However, in this study, only information on colloid attachment rate coefficient on to the grain surface was considered, assuming that deposition on grain surfaces and straining are two independent mechanisms. In another study, Torkzaban et al. (2008a) found that the retention of CML colloids to Ottawa sands is described using a one-site reversible kinetic model with blocking. In this study, only the values of rate coefficients of colloid attachment and detachment on to the grain surface were considered, thereby trying to estimate the values of deposition rate coefficients to an initially clean collector. Foppen et al. (2005) fitted the breakthrough data of *E. coli* using a two-site kinetic model, with site 1 being irreversible and site 2 being reversible. In this paper, the rate coefficient of attachment to only the irreversible site was considered, because most studies report that bacteria deposition on the grain surface is irreversible (Redman et al., 2004; Foppen et al., 2007; Torkzaban et al., 2008b; Kim and Walker, 2009; Bai et al., 2016).

The column-experimental papers selected to analyse the deposition of viruses, bacteria, GO NPs, Ag NPs, TiO_2 NPs, and CML colloids are listed in **Tables 1–6**, respectively, along with experimental conditions and mechanisms behind observed retention. The selected data includes 41 datasets (**Supplementary Table 1**) depicting various environmental conditions reported in five papers (Syngouna and Chrysikopoulos, 2012, 2013, 2015; Sasidharan et al., 2017a,b) for the transport of viruses such as MS2, PRD1, and ΦX174 through columns packed with quartz sand or glass beads (**Table 1**). **Table 1** shows that virus deposition on grain surface is described using a one-site reversible kinetic model for most experimental conditions. Six papers (Redman et al., 2004; Foppen et al., 2005, 2007; Torkzaban et al., 2008b; Kim and Walker, 2009; Bai et al., 2016) comprising 22 datasets (**Supplementary Table 2**) were selected for the analysis of deposition behavior of bacteria through sand and glass beads (**Table 2**). It is clear from **Table 2** that the deposition of bacteria on solid grains is predominantly described using a one-site irreversible kinetic model. The different types of bacteria considered in this study are *E. coli XL-1 Blue* (Kim and Walker, 2009), *E. coli D21g* (Redman et al., 2004; Foppen et al., 2005, 2007; Torkzaban et al., 2008b), and *Klebsiella Oxytoca* (Bai et al., 2016). The deposition trend vis-à-vis the physicochemical parameters for GO NPs through sand was analyzed using experimental results from three papers (Qi et al., 2014; Sun et al., 2015; Wang et al., 2017) constituting 31 datasets (**Table 3** and **Supplementary Table 3**). Similarly, for Ag and TiO_2 NPs, 21 datasets (Liang et al., 2013, 2020; Park et al., 2016) and 23 datasets (Fang et al., 2013; Bayat et al., 2015; Lv et al., 2016) were analyzed, as listed in **Tables 4**, **5**, respectively. The corresponding experimental datasets are listed in **Supplementary Tables 4, 5**, respectively. **Tables 3–5** show that for experimental conditions considered in this study, ENP deposition on grain surface is described using a one-site irreversible kinetic model. **Table 6** lists six selected papers (Li and Johnson, 2005; Li et al., 2005; Tong et al., 2005; Tong and Johnson, 2006; Johnson et al., 2007; Torkzaban et al., 2008a) comprising 50 datasets (**Supplementary Table 6**) used to understand the deposition behavior of CML colloids through glass beads and quartz sand. **Table 6** shows that deposition of CML colloids on solid grains is mostly described using a one-site reversible kinetic model.

For each of the colloid types considered in this study, selected column-experimental data were analyzed to develop empirical equations for attachment and detachment rate coefficients as a function of 11 dimensional parameters as given below:

$$k_a = f\left(\theta, \overline{v},\ d_{50}, a, I, \psi_c, \psi_g, H,\ T,\ \mu, \varepsilon\right) \tag{1}$$

$$k_d = g\left(\theta, \overline{v},\ d_{50}, a, I, \psi_c, \psi_g, H,\ T, \mu, \varepsilon\right) \tag{2}$$

where k_a $\left[\frac{1}{T}\right]$ *and* $k_d\left[\frac{1}{T}\right]$ are the rate coefficients for colloid attachment to and detachment from grain surfaces, respectively.

Dimensionless Parameters Controlling Colloid Deposition

Eleven dimensional parameters influencing colloid deposition were grouped into eight dimensionless parameters, including $\theta, Pe, A, \lambda^*, N_{E1}, N_{E2}, N_{DL},$ *and* H^*. Here, $Pe = \frac{\overline{v}d_{50}}{D_\infty}$ is the Peclet number, $D_\infty = \frac{k_BT}{6\pi\mu a}$ is the particle bulk diffusion coefficient, k_B is the Boltzmann constant, $A = \frac{a}{d_{50}}$ is the interception parameter, $\lambda^* = \frac{\lambda}{a}$ where λ is the characteristic wavelength of interaction ($\lambda = 100\,\text{nm}$), $N_{E1} = \frac{\pi\varepsilon\varepsilon_0 a\left({\psi_c}^2+{\psi_g}^2\right)}{k_BT}$

TABLE 1 | Experimental conditions in papers selected to analyse deposition of viruses.

References	Porous media	Virus	d_{50} (μm)	Colloid radius, *a* (nm)	Background electrolyte	Pore-water velocity, $\bar{v}$ (cm/min)	Porosity, θ	pH	Ionic strength, *I* (mM)	Zeta potential of colloid, ψ_c (mV)	Zeta potential of grain surface, ψ_g (mV)	Retention mechanism
Syngouna and Chrysikopoulos (2012)	Acid washed quartz sand	ΦX174, MS2	110, 520, 1,440	13 (ΦX174), 12.5 (MS2)	Phosphate buffer solution	0.39–1.31	0.39–0.43	7	1.2	−31.15 (ΦX174), −33.5 (MS2)	−53.03 to −64.72	Irreversible deposition
Syngouna and Chrysikopoulos (2013)	Acid washed glass beads	ΦX174, MS2	2,000	13 (ΦX174), 12.5 (MS2)	DDI water	0.38, 0.74, 1.21	0.42	7	0.1	−40.4 (*MS2*), −31.78 (ΦX174)	−54.6	Reversible deposition
Syngouna and Chrysikopoulos (2015)	Acid washed glass beads	ΦX174, MS2	2,000	13 (ΦX174), 12.5 (MS2)	DDI water	0.74	0.42	7	0.1	−31.78 (ΦX174), −40.4 (MS2)	−54.6	Reversible deposition
Sasidharan et al. (2017a)	Acid washed quartz sand	MS2, PRD1, ΦX174	210	14 (MS2), 14.5 (PRD1), 34 (ΦX174)	Storm water	0.07, 0.35	0.41	7, 7.3	0.002, 0.014	−12.6, −22.4 (MS2), −14.8, −23.3 (PRD1), −13.7, −23.8 (ΦX174)	−27.2, −31.5	Reversible deposition with blocking and inactivation
Sasidharan et al. (2017b)	Acid washed quartz sand	ΦX174, PRD1	210	13.5 (ΦX174), 31.5 (PRD1)	NaCl	0.007	0.4	5.5–5.8	10, 50	−17, −30 (ΦX174) −20, −33 (PRD1)	−15,-27	Two-site kinetic deposition: site 1- irreversible and site 2 - reversible

TABLE 2 | Experimental conditions in papers selected to analyse deposition of bacteria.

References	Porous media	Bacteria	d_{50} (μm)	Colloid radius, *a* (μm)	Background electrolyte	Pore-water velocity, $\bar{v}$ (cm/min)	Porosity, θ	pH	Ionic strength, *I* (mM)	Zeta potential of colloid, ψ_c (mV)	Zeta potential of grain surface, ψ_g (mV)	Retention mechanism
Redman et al. (2004)	Acid washed quartz sand	*E. coli D21g*	205	0.85	KCl	1.26	0.43	5.6–5.8	1, 3.2, 100	−21.5 to −61.4	−11.6 to −38.5	Irreversible deposition
Foppen et al. (2005)	Autoclaved quartz sand	*E. coli*	350	0.5	Tap water	0.01 to 0.05	0.4	7	10	−44.32	−32.08	2-site kinetic model: site 1- Irreversible deposition, and site 2: reversible deposition
Foppen et al. (2007)	Acid washed quartz sand	*E. coliD21g*	196	0.715	NaCl	2.784 to 3.25	0.439		5	−165.5	−78.3	2-site kinetic model: site 1- Irreversible deposition, and site 2: reversible deposition
Torkzaban et al. (2008b)	Acid washed quartz sand	*E. coliD21g*	205	0.92	KCl	0.66	0.43	5.6–5.8	10–100	−21 to −49	−11.2 to −22	Irreversible deposition with blocking
Kim and Walker (2009)	Acid washed quartz sand	*E. coli D21g, E.coli XL-1 Blue*	275	0.48 (*E. coli D21g*), 0.55 (*E. coli XL-1 Blue*)	KCl	1.02	0.46	5.6 –5.8	10, 20	−20.1 to −84.8 (*E. coli D21g*),−60.1 (*E. coli XL-1 Blue*)	−14 to −23	Irreversible deposition
Bai et al. (2016)	Autoclaved quartz sand	*E. coli, Klebsiella Oxytoca*	360, 900	0.55 (*E. coli*), 0.79 (*Klebsiella Oxytoca*)	NaCl	0.95, 1.077	0.34, 0.44	5.89	0. 1	−41 (*E. coli*), −33.2 (*Klebsiella Oxytoca*)	−12.5 to −39.6	Irreversible deposition

TABLE 3 | Experimental conditions in papers selected to analyse deposition of GO NPs.

References	Porous media	d_{50} (μm)	Colloid radius, *a* (nm)	Background electrolyte	Pore-water velocity, $\overline{v}$ (cm/min)	Porosity, θ	pH	Ionic strength, *I* (mM)	Zeta potential of colloid, ψ_c (mV)	Zeta potential of grain surface, ψ_g (mV)	Retention mechanism
Qi et al. (2014)	Quartz sand	255	125-210	NaCl	0.347, 0.694	0.42	4.8–5.8	10–50	−13.9 to −49	−30 to −75	Irreversible deposition with blocking and straining
Sun et al. (2015)	Quartz sand	150 - 925	295	NaCl	0.52	0.39–0.41	4.9–5.4	20	−30.73	−25.54 to −39.92	Irreversible deposition with blocking
Wang et al. (2017)	Quartz sand	350, 950	80-120	KCl	0.513, 0.606	0.33, 0.39	7	1, 10	−13.42 to −43.31	−23.63 to −48.88	Irreversible deposition with blocking

TABLE 4 | Experimental conditions in papers selected to analyse deposition of Ag NPs.

References	Porous media	d_{50} (μm)	Colloid radius, *a* (nm)	Background electrolyte	Pore-water velocity, $\overline{v}$ (cm/min)	Porosity, θ	pH	Ionic strength, *I* (mM)	Zeta potential of colloid, ψ_c (mV)	Zeta potential of grain surface, ψ_g (mV)	Retention mechanism
Liang et al. (2013)	Quartz sand	240-607	20.25-30	KNO_3	0.07–1.98	0.35–0.43	6–7	1–5	−3.2 to −16.9	−55	Irreversible deposition with blocking
Park et al. (2016)	Quartz sand	250	50	NaCl	1.11	0.370	7.3	10–100	−48.3 to −50.9	−60 to −65	Irreversible deposition with blocking and straining
Liang et al. (2020)	Quartz sand	510	40-60	KNO_3	1.40	0.500	4–9	5–50	−5.9 to −30.4	−17.7 to −57.4	Irreversible deposition with blocking

TABLE 5 | Experimental conditions in papers selected to analyse deposition of TiO_2 NPs.

References	Porous media	d_{50} (μm)	Colloid radius, *a* (nm)	Background electrolyte	Pore-water velocity, $\overline{v}$ (cm/min)	Porosity, θ	pH	Ionic strength, *I* (mM)	Zeta potential of colloid, ψ_c (mV)	Zeta potential of grain surface, ψ_g (mV)	Retention mechanism
Fang et al. (2013)	River sand	200	123.5–976	DI water	0.177–0.182	0.350	2.6–9.6	0.1–50	2.4 to −36.4	−22	Irreversible and reversible deposition with straining
Bayat et al. (2015)	Limestone sand	150	110–155	NaCl	0.65	0.340	6.2	0.003−500	1.6–9.1	23.1–33.1	Irreversible deposition with blocking
Lv et al. (2016)	Quartz sand	275–920	40-−0	NaCl	0.57	0.330	6.65	0.1–10	−29.9 to −38.1	−30.4 to −51.1	Irreversible deposition

TABLE 6 | Experimental conditions in papers selected to analyse deposition of CML colloids.

References	Porous media	d_{50} (μm)	Colloid radius, *a* (μm)	Background electrolyte	Pore-water velocity, $\overline{v}$ (cm/min)	Porosity, θ	pH	Ionic strength, *I* (mM)	Zeta potential of colloid, ψ_c (mV)	Zeta potential of grain surface, ψ_g (mV)	Retention mechanism
Li and Johnson (2005)	Acid washed quartz sand	510	0.5, 0.55	MOPS and $NaHCO_3$	0.139 to 0.556	0.360	6.92	1–20	−56.22 to −69.49	−31.73 to −99.74	Reversible deposition
Li et al. (2005)	Acid washed glass beads, Acid-washed quartz sand	510	0.55	NaCl	0.139, 0.278 (Acid-washed glass beads), 0.139 to 0.556 (Acid washed quartz sand)	0.37 (Acid-washed glass beads), 0.36 (Acid washed quartz sand)	6.92	20–50 (Acid washed SLGB), 3–20 (Acid washed quartz sand)	−48.5 to −70	−57.5 to −67.5 (Acid washed SLGB), −52.5 to −69.5 (Acid washed quartz sand)	Reversible deposition
Tong et al. (2005)	Acid washed glass beads	360	0.55	NaCl	0.139 and 0.278	0.38	6	6, 20	−55 to −60	−65 to −67.5	Reversible deposition
Tong and Johnson (2006)	Acid washed glass beads	510	0.5, 1	NaCl	0.139 to 0.556	0.38	2, 6.72	20, 50	−2.3 to −59	−10 to −69.5	Reversible deposition
Johnson et al. (2007)	Acid washed glass beads	360	0.55 and 2.85	NaCl	0.139 to 0.556	0.380	6	10–20	−15 to −70	−65 to −70	Reversible deposition
Torkzaban et al. (2008a)	Ottawa sand	240, 360	0.55	DI water	0.28 to 0.87	0.34	10	6, 60	−71 to −110	−70	Reversible deposition

represents the magnitudes of surface potentials of colloid and grains, ε_0 is the permittivity of vacuum, $N_{E2} = \frac{2\psi_c\psi_g}{(\psi_c{}^2+\psi_g{}^2)}$ represents the ratio of surface potentials of colloid and soil grains, $N_{DL} = \kappa a$ represents the ratio of colloid radius to Debye length, $\kappa = \sqrt{2000\, N_A I e^2/\varepsilon\varepsilon_0 k_B T}$ represents the inverse Debye length, N_A is the Avogadro number, e is the elementary charge of the particle, and $H^* = \frac{H}{k_B T}$ is the dimensionless Hamaker constant. The corresponding dimensionless rate coefficients are $Da_a = \frac{k_a d_{50}}{\bar{v}}$ and $Da_d = \frac{k_d d_{50}}{\bar{v}}$, where Da_a and Da_d are Damkohler numbers for colloid attachment to and detachment from grain surfaces, respectively. **Table 7** lists the range of values of dimensionless parameters for each colloid type for which empirical equations were developed in this study.

Variation of Dimensionless Deposition Rate Coefficients With Individual Parameters

The selected column-experimental data were analyzed to identify the trend and the relationship between Da_a and Da_d vis-à-vis each of the eight dimensionless parameters ($\theta, Pe,\ A,\ \lambda^*,\ N_{E1},\ N_{E2},\ N_{DL},\ and\ H^*$). **Figures 1A,B** show that a power-law relationship describes the variation of Da_a vs $Pe,\ A,\ and\ \theta$. Since the values of both N_{E1} *and* N_{E2} change with N_{DL}, the variation of Da_a vis-à-vis $N_{E1},\ N_{E2},\ and\ N_{DL}$ was plotted in **Figures 1C,D**, which show that a power-law relationship exists between them. **Figures 1E–G** show that the variation of Da_d with $N_{E1},\ N_{E2},\ N_{DL},\ and\ Pe$ can be described using a power-law function. No dataset showing the variation of Da_a or Da_d vs λ^* and $H^*$was found.

RESULTS AND DISCUSSION

Empirical Equations for Deposition Rate Coefficients of Colloids

Section Variation of Dimensionless Deposition Rate Coefficients With Individual Parameters and **Figures 1A–G** indicate that a power-law relationship describes the variation of Da_a and Da_d with respect to the various dimensionless parameters. Hence, in this study, the following empirical relationships between Da_a and Da_d vis-à-vis the eight dimensionless parameters were assumed for all the six different types of colloids considered:

$$ln\ Da_a = p_1 + p_2\ ln\theta + p_3 ln\ Pe + p_4 ln\ A + p_5\ ln\ \lambda^* + p_6 lnN_{E1} + p_7 lnN_{E2} + p_8 lnN_{DL} + p_9 lnH^* \quad (3)$$

$$ln\ Da_d = q_1 + q_2\ ln\theta + q_3 ln\ Pe + q_4 ln\ A + q_5\ ln\ \lambda^* + q_6 lnN_{E1} + q_7 lnN_{E2} + q_8 lnN_{DL} + q_9 lnH^* \quad (4)$$

where $p_1,\ p_2,\ \ldots.p_9$ and $q_1,\ q_2,\ \ldots.q_9$ are coefficients whose values were estimated using multiple-linear regression analysis. Empirical equations for deposition rate coefficients were developed separately for viruses, bacteria, GO NPs, Ag NPs, TiO_2 NPs, and CML colloids. As mentioned previously, in published literature, the deposition of viruses and CML colloids is described using a first-order reversible kinetic model, whereas that of bacteria and ENPs (GO NPs, Ag NPs, and TiO_2 NPs) is described using a first-order irreversible kinetic model. Hence, Equation 4 is applicable only to viruses and CML colloids. Estimated values of coefficients in empirical Equations 3, 4 for viruses, bacteria, GO NPs, Ag NPs, TiO_2 NPs, and CML colloids are given in **Table 8**.

Equations for the dimensionless deposition rate coefficients, i.e., Equations 3, 4, were converted into dimensional form, resulting in empirical equations for k_a and k_d in terms of 11 dimensional parameters ($\nu_m,\ \theta,\ d_{50}, \mu,\ a,\ I, \varepsilon,\ \psi_c, \psi_g,\ T,\ H$) as follows:

$$k_a = r_1 \bar{\nu}^{r_2} \theta^{r_3} d_{50}^{r_4} \mu^{r_5} a^{r_6} I^{r_7} \varepsilon^{r_8} (\psi_c^2 + \psi_g^2)^{r_9} (\psi_c\psi_g)^{r_{10}} T^{r_{11}} H^{r_{12}} \quad (5)$$

$$k_d = s_1 \bar{\nu}^{s_2} \theta^{s_3} d_{50}^{s_4} \mu^{s_5} a^{s_6} I^{s_7} \varepsilon^{s_8} (\psi_c^2 + \psi_g^2)^{s_9} (\psi_c\psi_g)^{s_{10}} T^{s_{11}} H^{s_{12}} \quad (6)$$

where $r_1,\ r_2,\ \ldots.r_{12}$ and $s_1,\ s_2,\ \ldots.s_{12}$ are the coefficients. The values of coefficients $r_2,\ r_3, \ldots r_{12}$ and $s_2,\ s_3,\ \ldots.s_{12}$ for all six colloidal types are listed in **Table 8**. The values of r_1 and s_1 were calculated in terms of various constants as given below:

$$r_1 = \exp(p_1) 6^{p_3} \pi^{p_3+p_6} .2000^{0.5p_8} .2^{p_7} .[N_A^{0.5p_8} .K_B^{-(p_3+p_6+0.5p_8+p_9)} .e^{p_8} .\varepsilon_0^{p_6-0.5p_8} .\lambda^{p_5}] \quad (7)$$

$$s_1 = \exp(q_1) 6^{q_3} \pi^{q_3+q_6} .2000^{0.5q_8} .2^{q_7} .[N_A^{0.5q_8} .K_B^{-(q_3+q_6+0.5q_8+q_9)} .e^{q_8} .\varepsilon_0^{q_6-0.5q_8} .\lambda^{q_5}] \quad (8)$$

The Hamaker constant was not found to have a significant impact on the model performance for Da_a and Da_d of viruses and was hence excluded from the model (**Table 8**). Similarly, porosity was found to have a negligible effect on the detachment rate coefficient of viruses and was thus excluded from the model (**Table 8**). Given the negligible variation in the value of the Hamaker constant for the experimental dataset of bacteria considered in this study (**Table 7**), it was not included in the model for Da_a (**Table 8**). Similarly, variation in the value of porosity is minimal for the experimental data of TiO_2 and was excluded from the model for Da_a (**Table 8**). Additionally, the Hamaker constant was found to have a negligible effect on the predicted value of Da_a for TiO_2 NPs and was also not included in the equation for Da_a (**Table 8**).

Figures 2A, **3**, **4**, **5A** compare the Da_a values predicted by the empirical equation developed in this study (Equation 3) with the corresponding values estimated by fitting the column-experimental data with appropriate models reported in the literature for viruses, bacteria, NPs, and CML colloids, respectively. It is apparent that the values of Da_a calculated using the empirical equations developed in this study match the corresponding values obtained from experimental data reported in literature reasonably well. The empirical equations were statistically significant with $p < .001$. **Figures 2B**, **5B** compare the Da_d values predicted by the empirical equation developed in this study (Equation 4) with the corresponding values obtained by fitting the column-experimental data with

TABLE 7 | Range of values of dimensionless parameters for various colloidal types.

Dimensionless parameter	Viruses	Bacteria	GO NP	Ag NP	TiO_2 NP	CML colloids
θ	0.39–0.43	0.36–0.46	0.33–0.42	0.35–0.5	0.33–0.35	0.34–0.38
Pe	15.28–21,344	2,790.11–460,446.38	1,825.37–110,054.95	746.46–34,083.95	3,332.19–27,272.75	21,345.51–442,439.06
A	6.25×10^{-6}-1.62×10^{-4}	6.17×10^{-4}-4.49×10^{-3}	8.42×10^{-5}-1.97×10^{-3}	3.71×10^{-5}-2×10^{-4}	4.63×10^{-5}-4.88×10^{-3}	0.001–0.008
λ^*	2.941–8	0.11–0.21	0.31–1.25	1.63–4.43	0.1–2.34	0.035–0.2
N_{E1}	3.83–36.01	280.31–13,243.60	37.07–552.36	12.43–188.31	45.92–906.65	71.369–11,344.873
N_{E2}	0.63–1.00	0.63–1.00	0.73–0.99	0.12–0.98	0.14–1	0.44–1
N_{DL}	0.065–23.071	18.25–952.91	8.24–235.90	2.34–51.79	0.63–714.82	51.789–1,320.15
H^*	1.05–1.82	1.58–1.70	1.55–2.59	0.59–13.09	2.47–3.39	0.936–1.68
Da_a	3.93×10^{-6}-1.11×10^{-1}	9.52×10^{-5}-2.8×10^{-2}	6.76×10^{-4}-3×10^{-2}	1.50×10^{-3}-1.06×10^{-1}	7.5×10^{-7}-0.013	1.08×10^{-4}-1.53×10^{-2}
Da_d	9.62×10^{-6}-0.092	0	0	0	0	2.07×10^{-5}-9.72×10^{-4}

appropriate models reported in the literature for viruses and CML colloids, respectively.

The empirical model predicted a positive trend for k_a with respect to mean pore-water velocity for all colloidal types, except TiO_2 NPs (Equation 5 and **Table 8**). This is consistent with experimental results reported in literature for viruses, bacteria, Ag NPs, GO NPs, and CML colloids (Hendry et al., 1999; Liang et al., 2013; Qi et al., 2014; Seetha et al., 2015b; Ma et al., 2017). The empirical model predicted a negative trend for k_a with respect to mean pore-water velocity for TiO_2 NPs, which is in line with the experimental data published by Toloni et al. (2014). Equation 6 and **Table 8** indicate that for viruses and CML colloids, k_d increases with velocity. This is in agreement with the experimental results reported by Chowdhury et al. (2011), Syngouna and Chrysikopoulos (2013), Tong and Johnson (2006), and Zhang et al. (2012).

The empirical model predicted a negative trend for k_a vis-à-vis grain size for all colloidal types, except bacteria (Equation 6 and **Table 8**). This is consistent with experimental studies conducted with *E. coli* (Foppen et al., 2007). In addition, for deposition of viruses and CML colloids, a positive correlation was found between k_d and grain size. As the grain size increases, the specific surface area of the porous medium decreases and the diffusion length to the grain surface increases. This results in lesser attachment with increasing grain size. This trend is consistent with CFT (Yao et al., 1971; Tufenkji and Elimelech, 2004) and experimental studies reported in literature for the deposition of bacteriophages, GO NPs, AgNPs, TiO_2 NPs, and CML colloids (Knappett et al., 2008; Kasel et al., 2013; Liang et al., 2013; Sun et al., 2015; Lv et al., 2016).

As viscosity increases, the particle diffusion coefficient decreases leading to lesser transport of particles from the liquid phase to the grain surface and from grain surface to the liquid phase. This caused a negative correlation between k_a and μ for viruses, AgNPs, TiO_2 NPs, and CML colloids (Equation 5 and **Table 8**). However, a positive correlation between k_a and μ was found for bacteria and GO NPs (Equation 5 and **Table 8**).

Diffusion coefficient of colloids increases with temperature, resulting in a higher rate of transfer of colloids to the grain surface, and hence increased deposition. This is consistent with the empirical equation for k_a (Equation 5) developed in this study for all colloid types, except bacteria. Kim and Walker (2009) performed experiments with different *E. coli* strains at varying temperatures and observed that temperature did not significantly affect bacterial deposition. They attributed the retention of bacteria to biological processes rather than transport processes.

Colloid deposition on grain surface increases with ionic strength because of decreasing electrostatic repulsive force between colloids and soil grains, due to their less negative surface potentials and compression of the double layer. This causes the attachment rate coefficient to increase with ionic strength (Chen and Zhu, 2004; Li et al., 2004, 2011; Johnson et al., 2007; Kim and Walker, 2009; Fang et al., 2013) and decrease with increasing values of $(\psi_c^2 + \psi_g^2)$ and $(\psi_c\psi_g)$. Furthermore, the detachment rate coefficient was expected to decrease with increase in ionic strength. This is in line with the trend predicted by the empirical equation for k_a vis-à-vis ionic strength (Equation 5 and **Table 8**) for all colloid types, except viruses. The opposite trend predicted by the empirical model for viruses may be due to the narrow range of ionic strength values in the data used for developing the empirical equation. Additionally, Equation 5 and **Table 8** show a negative trend between k_a vs $(\psi_c^2 + \psi_g^2)$ and $(\psi_c\psi_g)$ for all colloid types, except viruses and bacteria.

The empirical equation for k_a (Equation 5) predicts a negative trend with respect to particle radius for all colloid types, except viruses (**Table 8**). Since viruses are extremely small, diffusive transport dominates advective transport, and k_a (Equation 5) showed a positive trend with respect to particle radius due to increasing depth of the secondary minimum (**Table 8**). However, this is not true for NPs. NPs tend to aggregate, and the size of the aggregate is typically much larger than the size of individual NPs. Therefore, as particle size increases, the diffusion coefficient decreases, and the rate of transport of particles to the grain surface decreases (Tong and Johnson, 2006; Shen et al., 2008; Wang et al., 2012). As a result of their relatively large size, the k_a (Equation 5) for NPs, bacteria, and CML colloids showed a decreasing trend with increasing particle radius (**Table 8**).

Colloid deposition on grain surface increases with Hamaker constant due to an increase in attractive force between the colloid and soil grains. This is consistent with the empirical equation for

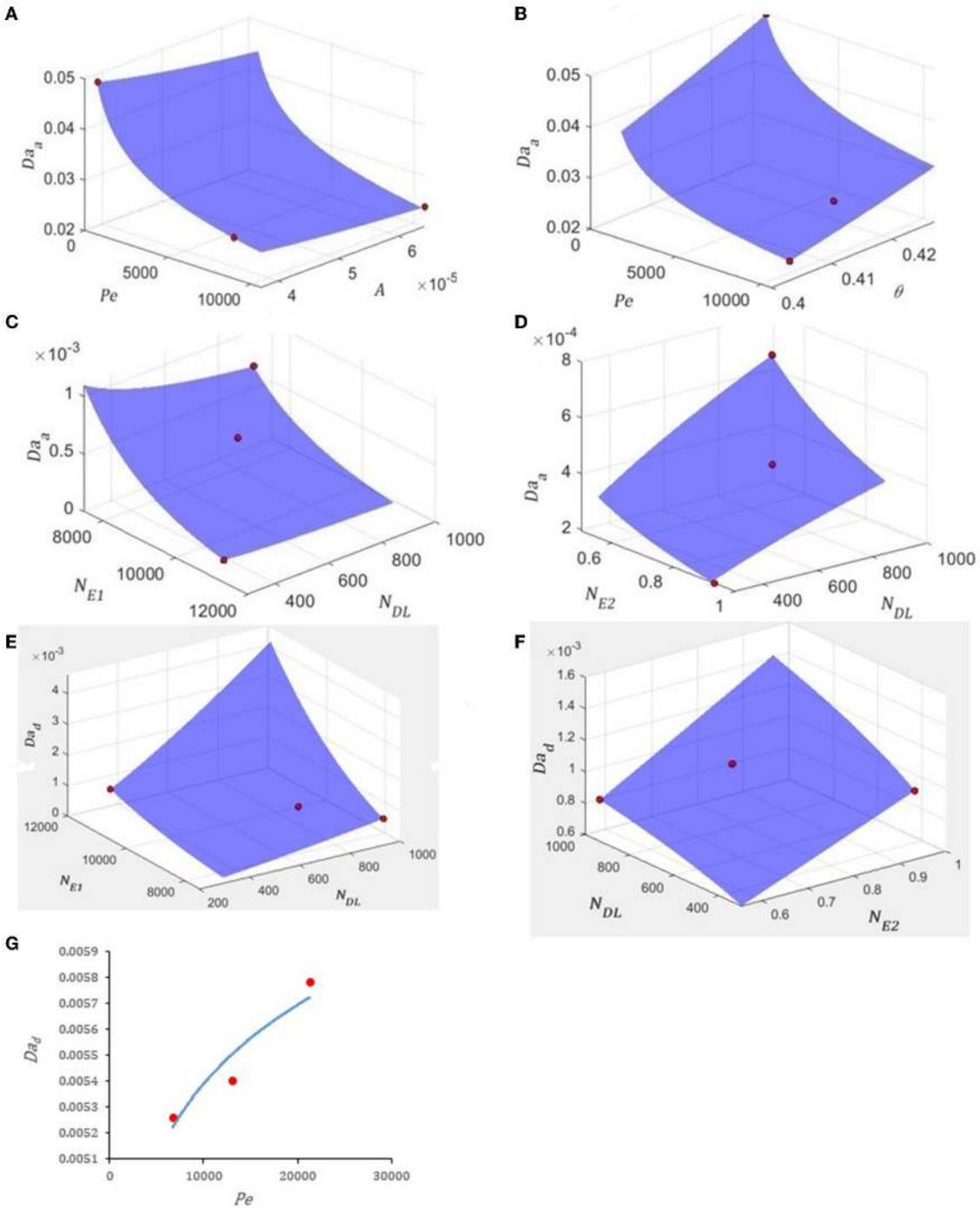

FIGURE 1 | Variation of **(A)** Da_a vs. Pe and A for Ag NPs, **(B)** Da_a vs. Pe and θ for Ag NPs, **(C)** Da_a vs. N_{E1} *and* N_{DL} for CML colloids, **(D)** Da_a *vs*. N_{E2} *and* N_{DL} for CML colloids, **(E)** Da_d vs. N_{E1} *and* N_{DL} for CML colloids, **(F)** Da_d vs. N_{DL} and N_{E2} for CML colloids, and **(G)** Da_d vs. Pe for $\Phi X174$. The fitted equations are **(A,B)** $Da_a = \theta^{2.926} Pe^{-0.199} A^{-0.08}$ and $R^2 = 1$, **(C,D)** $Da_a = N_{DL}{}^{0.3412} N_{E1}{}^{-1.129} N_{E2}{}^{-0.784}$ and $R^2 = 1$, **(E,F)** $Da_d = N_{E1}{}^{-0.797} N_{E2}{}^{1.247} N_{DL}{}^{0.116}$ and $R^2 = 1$, and **(G)** $Da_d = 0.0026\, Pe^{0.079}$ and $R^2 = 0.89$. The data (red circles) for this figure is from **(A,B)** Liang et al. (2013), **(C,D)** Johnson et al. (2007), **(E,F)** Johnson et al. (2007), and **(G)** Syngouna and Chrysikopoulos (2013). The values of the other dimensionless parameters are **(A,B)** $\lambda^* = 4.43$, $N_{E1} = 41.25$, $N_{E2} = 0.56$, $N_{DL} = 2.34$, and $H^* = 0.59$, **(C,D)** $\theta = 0.38$, $Pe = 221217.14$, $A = 0.0079$, $\lambda^* = 0.035$, and $H^* = 1.68$, **(E,F)** $\theta = 0.38$, $Pe = 221217.14$, $A = 0.0079$, $\lambda^* = 0.035$, and $H^* = 1.68$, and **(G)** $\theta = 0.42$, $A = 6.5\text{x}10^{-6}$, $\lambda^* = 7.69$, $N_{E1} = 31.74$, $N_{E2} = 0.96$, $N_{DL} = 0.43$, and $H^* = 1.82$.

TABLE 8 | Estimated values of coefficients in the empirical equations for the deposition rate coefficients of various colloids[a].

		Attachment rate coefficient						Detachment rate coefficient		
		Viruses	Bacteria	GO NPs	Ag NPs	TiO_2 NPs	CML colloids		Viruses	CML colloids
Coefficients of dimensionless empirical equation[b]	p_1	−9.73 (11.82)	−49.28 (10.12)	5.49 (4.60)	−9.70 (11.85)	−4.37 (3.36)	−19.37 (7.11)	q_1	−16.90 (5.40)	−5.44 (5.29)
	p_2	−9.82 (11.30)	−8.42 (2.22)	10.15 (2.29)	−2.05 (5.69)	0	−14.62 (3.96)	q_2	0	16.335 (3.24)
	p_3	−0.66 (0.31)	0.26 (0.24)	0.09 (0.19)	−0.24 (0.22)	−2.96 (0.44)	−0.58 (0.26)	q_3	0.11 (0.53)	−0.04 (0.20)
	p_4	−1.15 (0.54)	−3.87 (0.76)	0.71 (0.37)	−0.50 (0.89)	−3.38 (0.58)	0.10 (0.59)	q_4	−1.44 (1.45)	−1.78 (0.59)
	p_5	−4.66 (0.97)	−2.14 (1.16)	2.73 (0.66)	2.58 (1.88)	−5.62 (0.99)	0.94 (0.69)	q_5	−2.42 (3.29)	−0.73 (0.87)
	p_6	−1.36 (0.55)	−0.21 (0.23)	−0.62 (0.22)	−0.95 (0.23)	−0.23 (0.56)	−0.26 (0.16)	q_6	−0.24 (1.15)	0.49 (0.15)
	p_7	−2.24 (3.81)	−0.42 (1.67)	−0.26 (1.69)	−0.58 (0.29)	−0.11 (0.59)	−0.07 (1.15)	q_7	2.67 (5.24)	−3.28 (1.32)
	p_8	−1.12 (0.19)	1.34 (0.38)	1.33 (0.22)	1.22 (0.47)	0.28 (0.11)	1.63 (0.25)	q_8	0.67 (0.39)	−0.44 (0.18)
	p_9	0	0	4.06 (1.14)	0.11 (0.44)	0	0.42 (0.60)	q_9	0	−0.56 (0.38)
R^2		0.76	0.85	0.85	0.81	0.85	0.69		0.69	0.69
Coefficients of dimensional empirical equation[c]	r_2	0.34	1.26	1.09	0.76	−1.96	0.42	s_2	1.111	0.96
	r_3	−9.82	−8.42	10.15	−2.05	0	−14.62	s_3	0	16.34
	r_4	−0.50	3.13	−1.61	−0.75	−0.57	−1.68	s_4	0.556	0.74
	r_5	−0.66	0.26	0.09	−0.24	−2.96	−0.58	s_5	0.111	−0.04
	r_6	0.37	−0.35	−1.21	−3.05	−0.68	−0.06	s_6	1.522	−1.05
	r_7	−0.56	0.67	0.67	0.61	0.14	0.81	s_7	0.334	−0.22
	r_8	−0.79	−0.88	−1.28	−1.56	−0.37	−1.07	s_8	−0.570	0.71
	r_9	0.89	0.21	−0.36	−0.37	−0.12	−0.18	s_9	−2.903	3.77
	r_10	−2.24	−0.42	−0.26	−0.58	−0.11	−0.07	s_10	2.667	−3.28
	r_11	2.58	−0.72	−4.21	0.47	3.05	−0.40	s_11	−0.209	0.34
	r_12	0	0	4.06	0.11	0	0.42	s_12	0	−0.56

[a] *Values within brackets represent the standard error of the estimated coefficients.*
[b] *Coefficients in Equations 3, 4.*
[c] *Coefficients in Equations 5, 6.*

k_a (Equation 5), which predicted a positive trend with Hamaker constant for GO NPs, Ag NPs, and CML colloids (**Table 8**). The empirical equation for viruses, bacteria, and TiO_2 NPs did not include the Hamaker constant, as there is less variability in its value in the experimental dataset of these colloids considered in this study.

Comparison With Models in Literature

The performance of empirical equations for Da_a and Da_d developed in this study was compared with CFT. CFT (Yao et al., 1971) describes the deposition of colloids on grain surfaces under favorable conditions using a first-order irreversible kinetic model and the attachment rate coefficient was calculated as:

$$k_{a(CFT)} = \frac{3}{2}\frac{(1-\theta)}{d_{50}}\bar{v}\eta_0 \tag{9}$$

where η_0 is the single collector contact efficiency. Several theoretical expressions are available in the literature (Rajagopalan and Tien, 1976; Tufenkji and Elimelech, 2004; Ma et al., 2009; Nelson and Ginn, 2011) to calculate the value of η_0 for different collector geometries, range of parameter values and forces responsible for colloid attachment to the collector surface. Kamai et al. (2015) developed a semi-empirical expression for η_0 by regressing the correlation equation for η_0 proposed by Rajagopalan and Tien (1976) against the experimentally estimated values of η_0 to find the coefficients in the equation. This helps to account for additional factors such as surface heterogeneity of collectors, grain packing, incomplete mixing within and between pores, and particle aggregation, which were not accounted for in the mechanistic models for η_0. In this study, expressions for η_0 proposed by Tufenkji and Elimelech (2004) and Kamai et al. (2015) were used to predict the value of $k_{a(CFT)}$

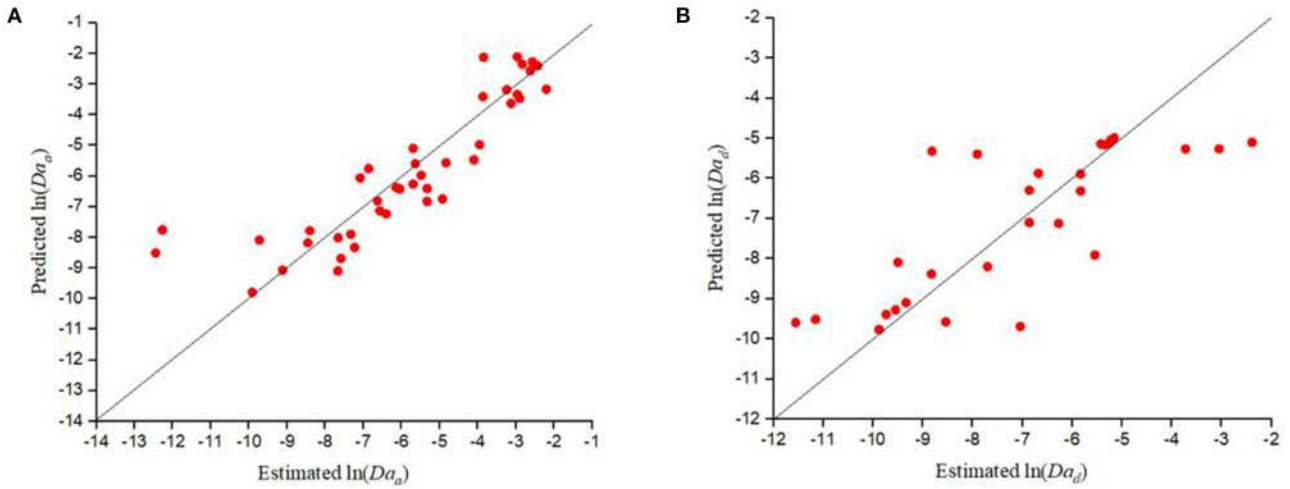

FIGURE 2 | Comparison of values of **(A)** Da_a ($R^2 = 0.76$) and **(B)** Da_d ($R^2 = 0.69$) predicted by the empirical equations developed in this study for viruses vs the corresponding estimated values reported in the literature (**Supplementary Table 1**) obtained by fitting column experimental data with a 1D mathematical model.

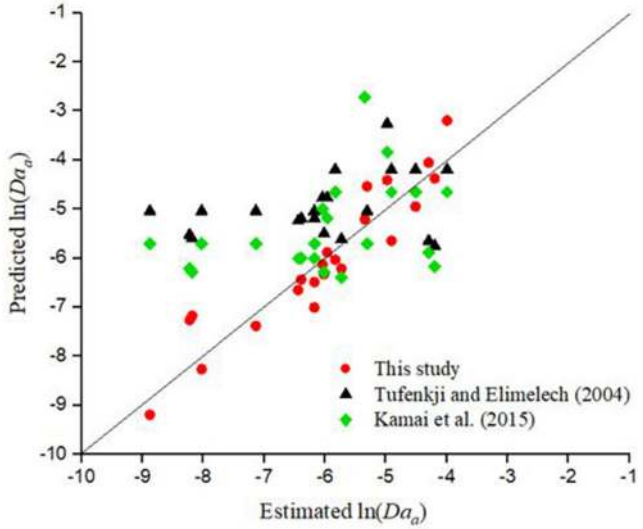

FIGURE 3 | Comparison of values of Da_a predicted by the empirical equation developed in this study for bacteria (red circles, $R^2 = 0.85$) vs the corresponding estimated values reported in the literature (**Supplementary Table 2**) obtained by fitting column experimental data with a 1D mathematical model. Also shown in the figure are the values of Da_a predicted by CFT with η_0 calculated using the model of Tufenkji and Elimelech (2004; black triangles, $R^2 = 0.103$), and Kamai et al. (2015; green diamonds, $R^2 = 0.156$).

using Equation 9. Tufenkji and Elimelech (2004) proposed the following equation for single collector contact efficiency ($\eta_{0(TE)}$):

$$\eta_{0(TE)} = 0.2779A_s^{0.33}a^{-0.796}\theta^{-0.715}{d_{50}}^{-0.634}\bar{\nu}^{-0.715}\mu^{-0.715}(k_BT)^{0.663}H^{0.052} + 1.1156\,A_s a^{1.425}\theta^{-0.125}{d_{50}}^{-1.675}\bar{\nu}^{-0.125}\mu^{-0.125}H^{0.125} + 0.4424a^{1.98}\,\theta^{-1.11}{d_{50}}^{0.24}\bar{\nu}^{-1.11}\mu^{-1.11}(k_BT)^{-0.053}H^{0.053}\left(\rho_p-\rho_f\right)^{1.11} \quad (10)$$

where A_s is the porosity dependent parameter in Happel's model, i.e., $A_s = 2(1-\gamma^5)/(2-3\gamma+3\gamma^5-2\gamma^6)$, $\gamma = (1-\theta)^{1/3}$, ρ_p [ML^{-3}] is the particle density, ρ_f [ML^{-3}] is the fluid density, and g [LT^{-2}] is the acceleration due to gravity.

Kamai et al. (2015) developed the following equation for single collector contact efficiency ($\eta_{0(KNNG)}$):

$$\eta_{0(KNNG)} = \gamma^2[0.1912A_s^{0.33}a^{-0.667}\theta^{-0.667}{d_{50}}^{-0.667}\bar{\nu}^{-0.667}\mu^{-0.667}(k_BT)^{0.667} + 0.1659A_s a^{1.144}\theta^{-0.1196}\,{d_{50}}^{-1.383}\bar{\nu}^{-0.1196}\mu^{-0.1196}H^{0.1196} + 1.858\times10^{-3}A_s a^{1.5327}\theta^{-1.045}{d_{50}}^{0.5573}\bar{\nu}^{-1.045}\left(\rho_p-\rho_f\right)^{1.045}\mu^{-1.045}] \quad (11)$$

The Damkohler number for attachment, predicted by CFT ($Da_{a(CFT)}$), was then calculated as $Da_{a(CFT)} = \frac{k_{a(CFT)}d_{50}}{\bar{\nu}}$. Since deposition to the grain surface was found to be irreversible in the case of bacteria and NPs, CFT was used to predict the corresponding values of Da_a for the experimental data considered in this study. **Figure 3** shows that CFT [with η_0 calculated using models proposed by Tufenkji and Elimelech (2004) and Kamai et al. (2015)] considerably overestimated the value of Da_a for the experimentally estimated ln (Da_a) values < -6 for the deposition of bacteria, and that the performance for η_0, calculated using the model suggested by Tufenkji and Elimelech (2004) ($p = .14$, $R^2 = 0.10$), is poor compared to the model proposed by Kamai et al. (2015) ($p = .07$, $R^2 = 0.16$). It is also apparent from **Figure 3** that in contrast to CFT, the empirical equation developed in this study is capable of estimating the Da_a values for bacteria more closely to the experimentally estimated Da_a values.

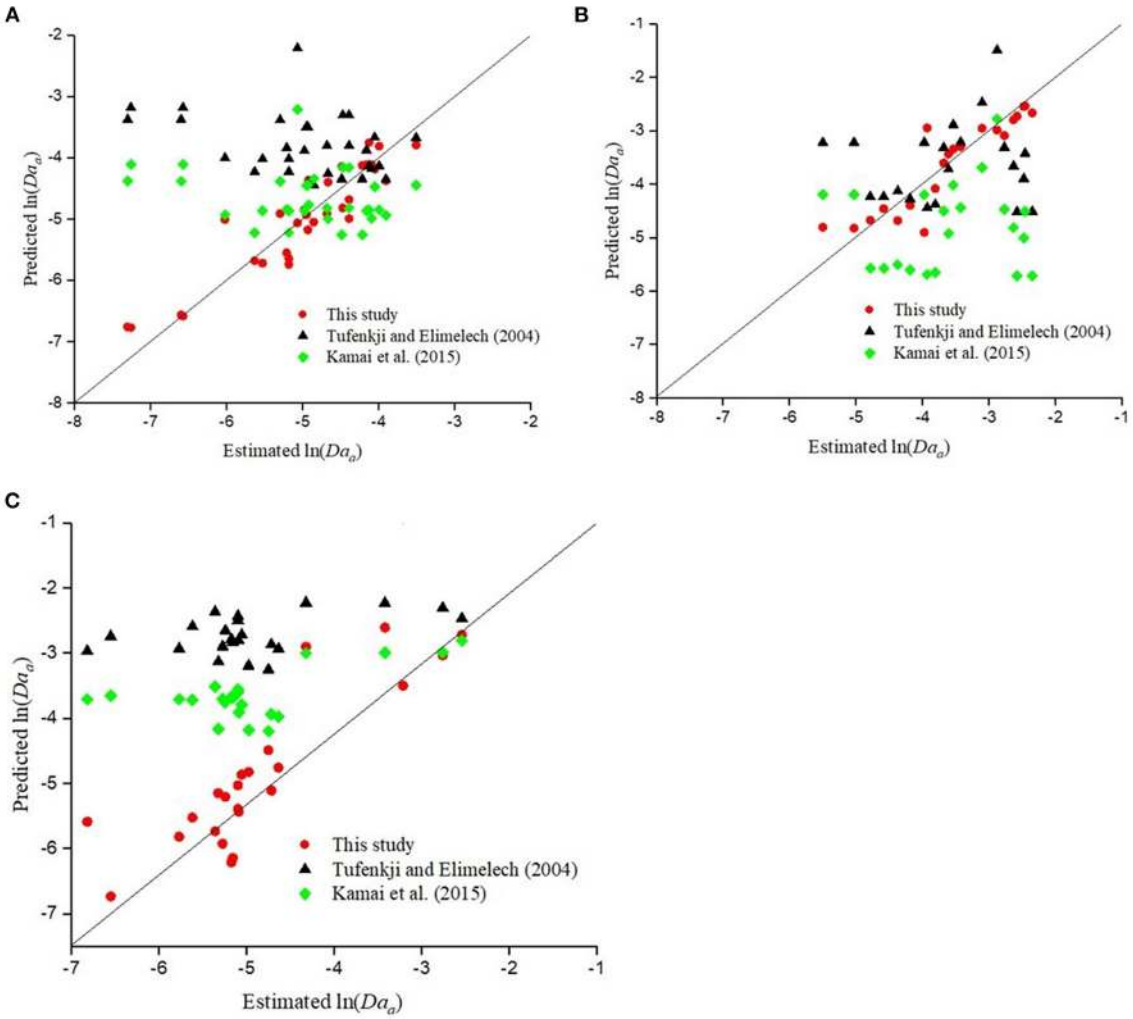

FIGURE 4 | Comparison of values of Da_a predicted by the empirical equation developed in this study for **(A)** GO NPs (red circles, $R^2 = 0.85$) **(B)** AgNPs (red circles, $R^2 = 0.824$) **(C)** TiO_2 NPs (red circles, $R^2 = 0.85$) vs. the corresponding estimated values reported in the literature (**Supplementary Tables 1–3**, respectively) obtained by fitting column experimental data with a 1D mathematical model. Also shown in the figure are the values of Da_a predicted by CFT with η_0 calculated using the model of Tufenkji and Elimelech (2004) for **(A)** GO NPs (black triangles, $R^2 = 0.139$), **(B)** AgNPs (black triangles, $R^2 = 0.009$), **(C)** TiO_2 NPs (black triangles, $R^2 = 0.289$) and Kamai et al. (2015) for **(A)** GO NPs (green diamonds, $R^2 = 0.078$), **(B)** AgNPs (green diamonds, $R^2 = 0.007$), **(C)** TiO_2 NPs (green diamonds, $R^2 = 0.366$).

Figure 4A compares the Da_a values predicted by CFT and the empirical model developed in this study (Equation 3 and **Table 8**) with the Da_a values estimated by fitting the experimental data with a one-dimensional model for the deposition of GO NPs. It is clear that the empirical model developed in this study is capable of predicting the Da_a values reasonably well, whereas the performance of CFT is poor ($p = .04 - .13$, $R^2 = 0.08 - 0.14$). **Figure 4B** shows that for Ag NPs, with η_0 calculated as per Kamai et al. (2015) ($p = .7$, $R^2 = 0.01$), CFT underestimated the value of Da_a whereas with η_0 calculated as per Tufenkji and Elimelech (2004) ($p = .68$, $R^2 = 0.01$), CFT overestimated the value of Da_a for $\ln(Da_a) < -4$. Overall, for the entire range of Da_a values for Ag NPs, the empirical equation developed in this study (Equation 3 and **Table 8**) performed reasonably well. A comparison between the Da_a values for TiO_2 NPs predicted by CFT and the empirical equation developed in this study (Equation 3 and **Table 8**) is shown in **Figure 4C**. It is clear that with η_0 calculated as per both Tufenkji and Elimelech (2004) ($p = .01$, $R^2 = 0.29$) and Kamai et al. (2015) ($p = .002$, $R^2 = 0.37$), CFT overestimated the Da_a values for TiO_2 NPs by several orders of magnitude, whereas the performance of the empirical equation developed in this study is reasonably satisfactory.

The deposition of CML colloids on grain surfaces is predominantly described using a reversible kinetic model, which indicates unfavorable conditions for deposition. The attachment rate coefficient of colloids under unfavorable conditions can be predicted using CFT by multiplying Equation 9 by α. Although a theoretical expression for α as a function of various physicochemical parameters is not available in literature, Bai and Tien (1999) developed an empirical equation for α as a function

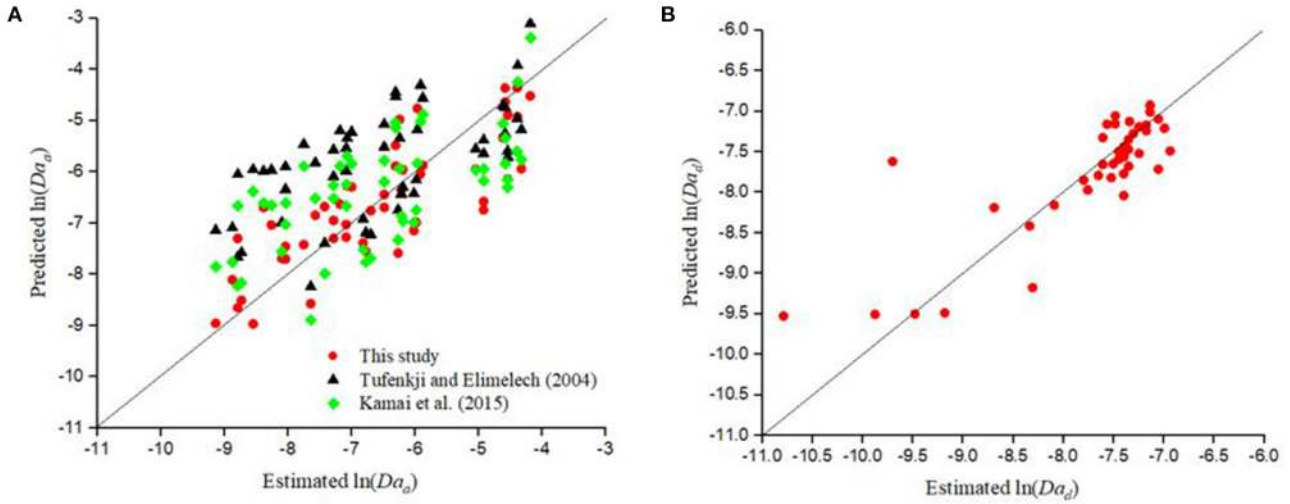

FIGURE 5 | Comparison of values of **(A)** Da_a (red circles, $R^2 = 0.69$) and **(B)** Da_d (red circles, $R^2 = 0.69$) values predicted by the empirical equations developed in this study for CML colloids vs the corresponding estimated values reported in the literature (**Supplementary Table 6**) obtained by fitting column experimental data with a 1D mathematical model. Also shown in **(A)** are the values of Da_a predicted by CFT with η_0 calculated using the model of Tufenkji and Elimelech (2004; black triangles, $R^2 = 0.39$) and Kamai et al. (2015; green diamonds, $R^2 = 0.41$) with the value of α calculated using the empirical equation developed by Bai and Tien (1999).

of various physicochemical parameters for the deposition of polystyrene latex particles to glass beads, which is given below:

$$\alpha = 2.989[{N_A}^{0.676} e^{1.352}\ {k_B}^{-0.676}\ {\varepsilon_0}^{-0.9881}]\varepsilon^{-0.9881} (T)^{-0.676}(\psi_c^2 + \psi_g^2)^{-3.8231}\ (\psi_c\psi_g)^{3.511} I^{0.676} \mu^{-0.391}\bar{\nu}^{-0.391} a^{0.2579}\theta^{-10.391} H^{0.7031} \quad (12)$$

Figure 5A shows the Da_a values for CML colloids predicted by CFT with η_0 calculated using the expression derived by either Tufenkji and Elimelech (2004) or Kamai et al. (2015) and α using Equation 12. CFT overestimated ($p < .001$, $R^2 = 0.39 - 0.41$) the values of Da_a and its performance was poorer than the empirical equation developed in this study (Equation 3 and **Table 8**).

Figures 3, **4A,C**, **5** show that CFT overpredicted the deposition of bacteria, GO NPs, TiO_2 NPs, and CML colloids, respectively, indicating that the attachment rate coefficient predicted by CFT must be multiplied by the sticking efficiency to make reasonable predictions. Sticking efficiency is calculated as the ratio of experimentally estimated Da_a and $Da_{a(CFT)}$. Hence, for the dataset given in **Supplementary Tables 1–3**, **5**, **6**, α values were calculated separately using the η_0 expressions proposed by Tufenkji and Elimelech (2004) or Kamai et al. (2015), and then used to find an empirical expression between α and eight dimensionless parameters for viruses, bacteria, GO NPs, TiO2 NPs, and CML colloids, as given below:

$$ln\,\alpha = l_1 + l_2\, ln\theta + l_3\, ln\, Pe + l_4 \ln\, A + l_5\, ln\,\lambda^* + l_6\, lnN_{E1} + l_7\, lnN_{E2} + l_8\, lnN_{DL} + l_9\, lnH^* \quad (13)$$

where $l_1, l_2 \ldots..l_9$ are coefficients whose values are estimated using multiple-linear regression analysis. Two separate equations for α are proposed in this study for each colloid type, corresponding to the calculation of η_0 using expressions proposed by either Tufenkji and Elimelech (2004) or Kamai et al. (2015). For certain data points in **Supplementary Tables 1–3**, **5**, **6**, α was found to be greater than one, and such data points were excluded from the regression analysis. The values of coefficients $l_1, l_2 \ldots..l_9$ for various colloidal types are given in **Table 9**. CFT underpredicted the deposition of Ag NPs (**Figure 4B**), indicating that CFT is not suitable for predicting the attachment rate coefficient of Ag NPs. The general form of the equation for α in terms of dimensional parameters is:

$$\alpha = m_1\bar{\nu}^{m_2}\theta^{m_3} d_{50}^{m_4}\mu^{m_5} a^{m_6} I^{m_7}\varepsilon^{m_8}(\psi_c^2 + \psi_g^2)^{m_9} (\psi_c\psi_g)^{m_{10}} T^{m_{11}} H^{m_{12}} \quad (14)$$

where $m_1, m_2, \ldots. m_{12}$ are the coefficients. **Table 9** lists the values of coefficients $m_2, m_3 \ldots. m_{12}$ for various colloid types. The value of m_1 can be calculated as:

$$m_1 = \exp(l_1) 6^{l_3}\pi^{l_3+l_6} 2000^{0.5l_8} 2^{l_7}[N_A^{0.5l_8} K_B^{-(l_3+l_6+0.5l_8+l_9)} e^{l_8}\varepsilon_0^{l_6-0.5l_8}\lambda^{l_5}] \quad (15)$$

Figure 6 compares the values of α predicted by the empirical model (Equation 13 and **Table 9**) developed in this study for various colloid types compared to the estimated values of α obtained from CFT using the expressions for η_0 proposed by Tufenkji and Elimelech (2004) and Kamai et al. (2015). The empirical model was found to predict the sticking efficiency reasonably well for various colloids. A comparison between the Da_a values predicted by CFT by multiplying Equation 9 by α calculated using the empirical model developed in this study (Equation 13 and **Table 9**), and the corresponding estimated

TABLE 9 | Estimated values of coefficients in the empirical equations of α for various colloids[a].

		η_0 expression by Tufenkji and Elimelech (2004)					η_0 expression by Kamai et al. (2015)				
		Viruses	**Bacteria**	**GO NPs**	**TiO_2 NPs**	**CML colloids**	**Viruses**	**Bacteria**	**GO NPs**	**TiO_2 NPs**	**CML colloids**
Coefficients of dimensionless empirical equation[b]	l_1	−9.81 (12.85)	−56.17 (23.66)	−5.68 (34.95)	−64.14 (19.46)	−29.23 (6.06)	−12.95 (12.95)	−47.73 (24.73)	−9.84 (45.74)	−52.54 (10.62)	−19.22 (6.25)
	l_2	−7.36 (12.21)	−8.19 (2.44)	8.20 (16.49)	−56.41 (14.84)	−21.53 (3.22)	−8.08 (12.05)	−7.30 (2.54)	5.79 (21.75)	−45.81 (23.83)	−18.66 (4.23)
	l_3	0.03 (0.43)	1.08 (0.35)	0.72 (0.23)	−4.42 (1.34)	−0.58 (0.23)	−0.35 (0.48)	1.04 (0.37)	0.35 (0.23)	−4.41 (4.84)	−0.65 (0.22)
	l_4	−0.97 (0.61)	−4.01 (2.48)	−0.33 (2.70)	−4.80 (1.35)	−1.05 (0.57)	−1.45 (0.66)	−3.25 (2.59)	−1.02 (3.52)	−4.61 (4.90)	−0.68 (0.58)
	l_5	−4.03 (1.12)	−0.27 (3.52)	2.55 (2.41)	−8.49 (2.46)	−0.15 (0.77)	−4.31 (1.17)	0.73 (3.66)	2.93 (2.81)	−8.32 (8.94)	0.03 (0.82)
	l_6	−1.49 (0.61)	0.25 (0.23)	−0.78 (0.59)	−0.07 (0.18)	−0.39 (0.18)	−1.09 (0.65)	0.20 (0.24)	−0.67 (0.71)	−0.64 (0.64)	−0.62 (0.52)
	l_7	−0.97 (5.17)	1.27 (3.93)	−2.51 (2.35)	−1.30 (0.09)	−0.33 (0.84)	−0.77 (5.30)	0.63 (4.13)	−1.18 (2.82)	0.53 (0.33)	−0.68 (0.80)
	l_8	−1.06 (0.42)	1.63 (0.88)	1.49 (0.35)	0.23 (0.05)	1.32 (0.19)	−0.98 (0.43)	1.45 (0.92)	1.71 (0.46)	0.34 (0.19)	1.04 (0.19)
	l_9	1.13 (5.04)	1.15 (6.17)	1.73 (9.04)	2.13 (4.14)	1.47 (0.45)	2.32 (5.15)	3.24 (11.21)	1.06 (12.06)	6.84 (15.02)	1.73 (0.42)
R^2		0.70	0.83	0.93	0.99	0.79	0.68	0.82	0.88	0.92	0.75
Coefficients of dimensional empirical equation[c]	m_1	0.03	1.08	0.72	−4.42	−0.58	−0.35	1.04	0.35	−4.41	−0.65
	m_2	−7.36	−8.19	8.20	−56.41	−21.53	−8.08	−7.30	5.79	−45.81	−18.66
	m_3	0.99	5.10	1.05	0.38	0.47	1.10	4.29	1.37	0.20	0.04
	m_4	0.03	1.08	0.72	−4.42	−0.58	−0.35	1.04	0.35	−4.41	−0.65
	m_5	0.54	−0.78	−1.44	−0.55	−0.55	0.44	−1.30	−2.56	−0.99	−0.93
	m_7	−0.53	0.82	0.75	0.12	0.66	−0.49	0.72	0.86	0.17	0.52
	m_8	−0.96	−0.57	−1.53	−0.18	−1.05	−0.60	−0.52	−1.53	−0.81	−1.14
	m_9	−2.46	−1.02	1.73	1.24	−0.06	−0.32	−0.43	0.50	−1.17	0.07
	m_{10}	0.97	1.27	−2.51	−1.30	−0.33	−0.77	0.63	−1.18	0.53	−0.68
	m_{11}	0.86	−3.30	−2.42	2.23	−1.16	−0.39	−5.20	−1.59	−1.97	−0.99
	m_{12}	1.13	1.15	1.73	2.13	1.47	2.32	3.24	1.06	6.84	1.73

[a] *Values within brackets represent the standard error of the estimated coefficients.*
[b] *Coefficients in Equation 13.*
[c] *Coefficients in Equation 14.*

values obtained from experimental data reported in the literature for viruses, bacteria, GO NPs, TiO_2 NPs, and CML colloids, is shown in **Supplementary Figure 1**. It is clear from **Figures 3–5** and **Supplementary Figure 1** that the performance of CFT in predicting the Da_a values improved ($p < .001$, $R^2 = 0.65 - 0.95$) when $Da_{a(CFT)}$ (Equation 9) was multiplied by α calculated using the empirical model developed in this study (Equation 13 and **Table 9**).

CONCLUSION

Empirical equations to estimate the first-order deposition rate coefficients of viruses, bacteria, GO NPs, Ag NPs, TiO_2 NPs, and CML colloids to grain surfaces were developed as a function of 11 physicochemical parameters, including porosity, mean pore-water velocity, median grain size, colloid radius, solution ionic strength, surface potentials of colloids and grains, Hamaker constant, temperature, viscosity of water, and dielectric constant. Deposition of bacteria, GO NPs, Ag NPs, and TiO_2 NPs was described using an irreversible kinetic model, whereas the deposition of viruses and CML colloids was described using a reversible kinetic model. It was found that a power-law relation describes the variation of deposition rate coefficients with respect to various physicochemical parameters. The empirical model developed in this study was found to predict the attachment and detachment rate coefficients of various colloids reasonably well, and its performance was found to be better than that of CFT. The discrepancy between the simulated and expected trend of deposition rate coefficients of viruses and bacteria vis-à-vis certain parameters may be due to: (a) the broad range of values of parameters and associated deposition rate coefficients depicting varying experimental conditions simulated in this study, (b) different sources of soil used in different studies, leading to differences in grain size distribution and surface

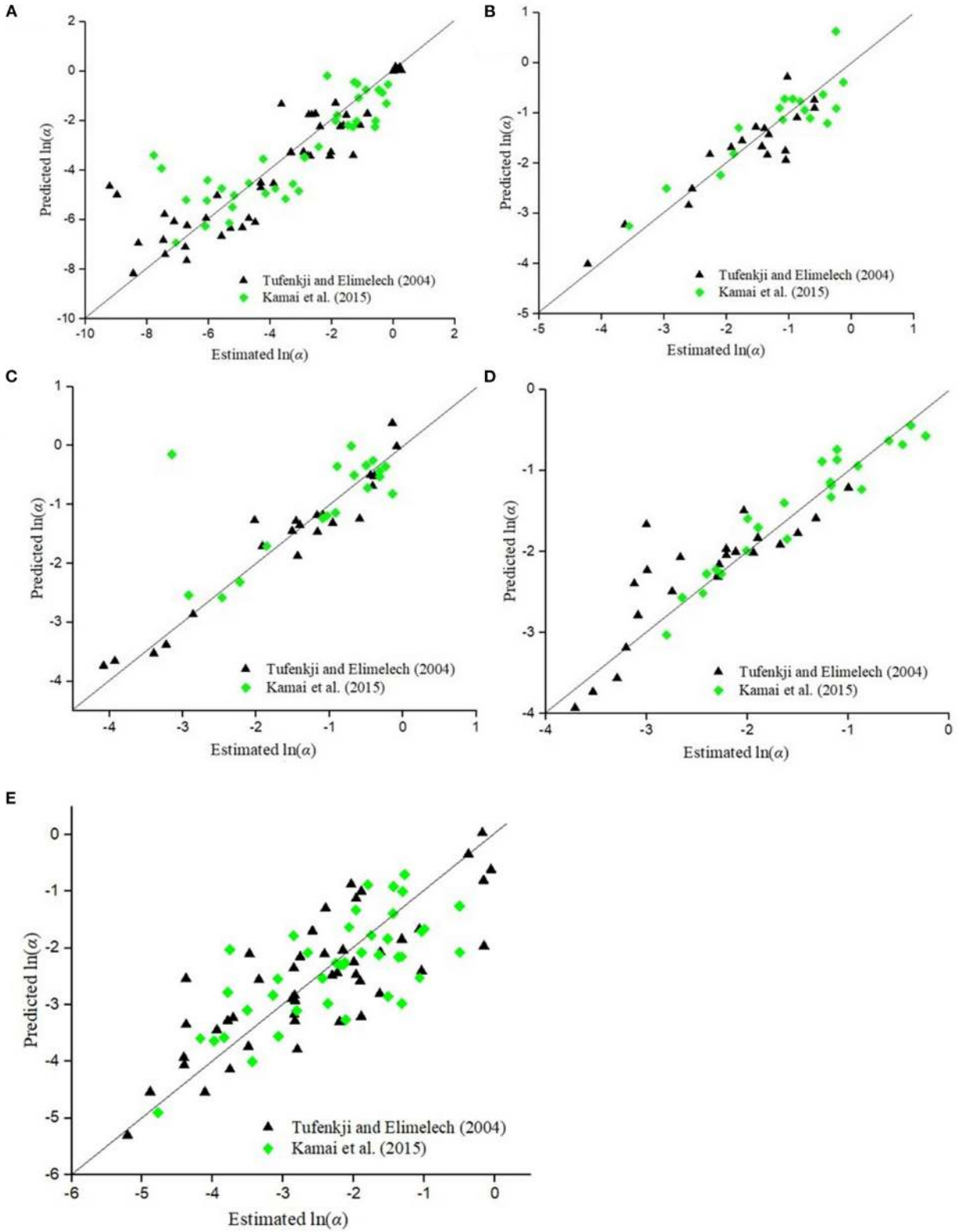

FIGURE 6 | Comparison of α values predicted by the empirical model Equation (13) developed in this study with the corresponding values calculated as the ratio of experimentally estimated Da_a and $Da_{a(CFT)}$ for η_0 expressions proposed by Tufenkji and Elimelech (2004) and Kamai et al. (2015) for **(A)** viruses, **(B)** bacteria, **(C)** GO NPs, **(D)** TiO_2 NPs, and **(E)** CML colloids.

properties of soils, (c) differences in the surface properties of synthetic colloids and biocolloids used in different studies, and (d) biological factors that are not accounted for in this study. Although the model is expected to perform well in terms of predicting the rate coefficients for an unknown dataset if the parameter values, soil type, and mineral composition of soil satisfy the conditions considered in model formulation, its performance outside the considered parameter range, and in particular, for soils with different mineral compositions, needs to be explored further. Empirical expressions were developed for the sticking efficiency of viruses, bacteria, GO NPs, TiO_2 NPs, and CML colloids as a function of various physicochemical parameters, which were found to improve the performance of CFT in predicting the attachment rate coefficients of these colloids.

DATA AVAILABILITY STATEMENT

The original contributions presented in the study are included in the article/**Supplementary Material**, further inquiries can be directed to the corresponding author/s.

AUTHOR CONTRIBUTIONS

YK: conceptualization, methodology, data curation, formal analysis, and writing—original draft. NS: conceptualization, methodology, writing—review and editing, and supervision. All authors contributed to the article and approved the submitted version.

FUNDING

The authors acknowledge the funding received from Department of Science and Technology, Government of India [grant number: DST/TM/WTI/WIC/2K17/100(G) 2] for carrying out this research.

SUPPLEMENTARY MATERIAL

The Supplementary Material for this article can be found online at: https://www.frontiersin.org/articles/10.3389/frwa.2022.827923/full#supplementary-material

REFERENCES

Bai, H., Cochet, N., Drelich, A., Pauss, A., and Lamy, E. (2016). Comparison of transport between two bacteria in saturated porous media with distinct pore size distribution. *RSC Adv.* 6, 14602–14614. doi: 10.1039/C5RA21695H

Bai, R., and Tien, C. (1999), Particle deposition under unfavorable surface interactions. *J. Colloid Interface Sci.*. 218, 488–499. doi: 10.1006/jcis.1999.6424

Bayat, A. E., Junin, R., Derahman, M. N., and Samad, A. A. (2015). TiO_2 nanoparticle transport and retention through saturated limestone porous media under various ionic strength conditions. *Chemosphere* 134, 7–15. doi: 10.1016/j.chemosphere.2015.03.052

Bradford, S. A., Simunek, J., Bettahar, M., Van Genuchten, M. T., and Yates, S. R. (2003). Modeling colloid attachment, straining, and exclusion in saturated porous media. *Environ. Sci. Technol.* 37, 2242–2250. doi: 10.1021/es025899u

Chen, G., and Zhu, H. (2004). Bacterial deposition in porous medium as impacted by solution chemistry. *Res. Microbiol.* 155, 467–474. doi: 10.1016/j.resmic.2004.02.004

Chowdhury, I., Hong, Y., Honda, R. J., and Walker, S. L. (2011). Mechanisms of TiO_2 nanoparticle transport in porous media: role of solution chemistry, nanoparticle concentration, and flowrate. *J. Colloid Interface Sci.* 360, 548–555. doi: 10.1016/j.jcis.2011.04.111

Chrysikopoulos, C. V., and Aravantinou, A. F. (2014). Virus attachment onto quartz sand: Role of grain size and temperature. *J. environ. Chem. Eng.* 2, 796–801.

Chu, Y., Jin, Y., Baumann, T., and Yates, M. V. (2003). Effect of soil properties on saturated and unsaturated virus transport through columns. *J. Environ. Qual.* 32, 2017–2025. doi: 10.2134/jeq2003.2017

Elimelech, M. (1992). Predicting collision efficiencies of colloidal particles in porous media. *Water Resour. Res.* 26, 1–8, doi: 10.1016/0043-1354(92)90104-C

Fang, J., Xu, M., Wang, D., Wen, B., and Han, J. Y. (2013). Modeling the transport of TiO_2 nanoparticle aggregates in saturated and unsaturated granular media: effects of ionic strength and pH. *Water Res.* 47, 1399–1408. doi: 10.1016/j.watres.2012.12.005

Foppen, J. W., Van Herwerden, M., and Schijven, J. (2007). Measuring and modelling straining of *Escherichia coli* in saturated porous media. *J. Contaminant Hydrol.* 93, 236–254. doi: 10.1016/j.jconhyd.2007.03.001

Foppen, J. W. A., Mporokoso, A., and Schijven, J. F. (2005). Determining straining of *Escherichia coli* from breakthrough curves. *J. Contaminant Hydrol.* 76, 191–210. doi: 10.1016/j.jconhyd.2004.08.005

Hedayati, M., Sharma, P., Katyal, D., and Fagerlund, F. (2016). Transport and retention of carbon-based engineered and natural nanoparticles through saturated porous media. *J. Nanoparticle Res.* 18, 1–11. doi: 10.1007/s11051-016-3365-6

Hendry, M. J., Lawrence, J. R., and Maloszewski, P. (1999). Effects of velocity on the transport of two bacteria through saturated sand. *Ground Water* 37, 103–112. doi: 10.1111/j.1745-6584.1999.tb00963.x

Jewett, D. G., Hilbert, T. A., Logan, B. E., Arnold, R. G., and Bales, R. C. (1995). Bacterial transport in laboratory columns and filters: influence of ionic strength and pH on collision efficiency. *Water Res.* 29, 1673–1680. doi: 10.1016/0043-1354(94)00338-8

Johnson, W. P., Li, X., and Assemi, S. (2007). Deposition and re-entrainment dynamics of microbes and non-biological colloids during non-perturbed transport in porous media in the presence of an energy barrier to deposition. *Adv. Water Resour.* 30, 1432–1454. doi: 10.1016/j.advwatres.2006.05.020

Kamai, T., Nassar, M. K., Nelson, K. E., and Ginn, T. R. (2015). Colloid filtration prediction by mapping the correlation-equation parameters from transport experiments in porous media. *Water Resour. Res.* 51, 8995–9012. doi: 10.1002/2015WR017403

Kasel, D., Bradford, S. A., Šimunek, J., Heggen, M., Vereecken, H., and Klumpp, E. (2013). Transport and retention of multi-walled carbon nanotubes in saturated porous media: effects of input concentration and grain size. *Water Res.* 47, 933–944. doi: 10.1016/j.watres.2012.11.019

Keller, A. A., Sirivithayapakorn, S., and Chrysikopoulos, C. V. (2004). Early breakthrough of colloids and bacteriophage MS2 in a water-saturated sand column. *Water Resour. Res.* 40, 1–11. doi: 10.1029/2003WR002676

Kim, H. N., and Walker, S. L. (2009). Escherichia coli transport in porous media: influence of cell strain, solution chemistry, and temperature. *Colloid. Surf. B Biointerfaces* 71, 160–167. doi: 10.1016/j.colsurfb.2009.02.002

Knappett, P. S., Emelko, M. B., Zhuang, J., and McKay, L. D. (2008). Transport and retention of a bacteriophage and microspheres in saturated, angular porous media: effects of ionic strength and grain size. *Water Res.* 42, 4368–4378. doi: 10.1016/j.watres.2008.07.041

Li, X., and Johnson, W. P. (2005). Nonmonotonic variations in deposition rate coefficients of microspheres in porous media under unfavorable deposition conditions. *Environ. Sci. Technol.* 39, 1658–1665. doi: 10.1021/es048963b

Li, X., Scheibe, T. D., and Johnson, W. P. (2004). Apparent decreases in colloid deposition rate coefficients with distance of transport under unfavorable deposition conditions: a general phenomenon. *Environ. Sci. Technol.* 38, 5616–5625. doi: 10.1021/es049154v

Li, X., Zhang, P., Lin, C. L., and Johnson, W. P. (2005). Role of hydrodynamic drag on microsphere deposition and re-entrainment in porous media under unfavorable conditions. *Environ. Sci. Technol.* 39, 4012–4020. doi: 10.1021/es048814t

Li, Z., Sahle-Demessie, E., Hassan, A. A., and Sorial, G. A. (2011). Transport and deposition of CeO_2 nanoparticles in water-saturated porous media. *Water Res.* 45, 4409–4418. doi: 10.1016/j.watres.2011.05.025

Liang, Y., Bradford, S. A., Simunek, J., Vereecken, H., and Klumpp, E. (2013). Sensitivity of the transport and retention of stabilized silver nanoparticles to physicochemical factors. *Water Res.* 47, 2572–2582. doi: 10.1016/j.watres.2013.02.025

Liang, Y., Zhou, J., Dong, Y., Klumpp, E., Šimunek, J., and Bradford, S. A. (2020). Evidence for the critical role of nanoscale surface roughness on the retention and release of silver nanoparticles in porous media. *Environ. Poll.* 258:113803. doi: 10.1016/j.envpol.2019.113803

Lv, X., Gao, B., Sun, Y., Dong, S., Wu, J., Jiang, B., et al. (2016). Effects of grain size and structural heterogeneity on the transport and retention of nano-TiO_2 in saturated porous media. *Sci. Tot. Environ.* 563, 987–995. doi: 10.1016/j.scitotenv.2015.12.128

Ma, E., Ouahbi, T., Wang, H., Ahfir, N. D., Alem, A., and Hammadi, A. (2017). Modeling of retention and re-entrainment of mono- and poly-disperse particles: effects of hydrodynamics, particle size and interplay of different-sized particles retention. *Sci. Tot. Environ.* 596–597, 222–229. doi: 10.1016/j.scitotenv.2017.03.254

Ma, H., Pedel, J., Fife, P., and Johnson, W. P. (2009). Hemispheres-in-cell geometry to predict colloid deposition in porous media. *Environ. Sci. Technol.* 43, 8573–8579. doi: 10.1021/es901242b

Mitropoulou, P. N., Syngouna, V. I., and Chrysikopoulos, C. V. (2013). Transport of colloids in unsaturated packed columns: role of ionic strength and sand grain size. *Chemical Eng. J.* 232, 237–248. doi: 10.1016/j.cej.2013.07.093

Nelson, K. E., and Ginn, T. R. (2011). New collector efficiency equation for colloid filtration in both natural and engineered flow conditions. *Water Resour. Res.* 47:9587. doi: 10.1029/2010WR009587

Park, C. M., Heo, J., Her, N., Chu, K. H., Jang, M., and Yoon, Y. (2016). Modeling the effects of surfactant, hardness, and natural organic matter on deposition and mobility of silver nanoparticles in saturated porous media. *Water Res.* 103, 38–47. doi: 10.1016/j.watres.2016.07.022

Park, Y., Atwill, E. R., Ho, L., Packman, A. I., and Harter, T. (2012). Deposition of cryptosporidium parvum Oocysts in porous media: a synthesis of attachment efficiencies measured under varying environmental conditions. *Environ. Sci. Technol.* 46, 9491–9500. doi: 10.1021/es300564w

Qi, Z., Zhang, L., Wang, F., Hou, L., and Chen, W. (2014). Factors controlling transport of graphene oxide nanoparticles in saturated sand columns. *Environ. Toxicol. Chem.* 33, 998–1004. doi: 10.1002/etc.2525

Rajagopalan, R., and Tien, C. (1976). Trajectory analysis of deep-bed filtration with the sphere-in-cell porous media model. *AIChE J.* 22, 523–533. doi: 10.1002/aic.690220316

Redman, J. A., Walker, S. L., and Elimelech, M. (2004). Bacterial adhesion and transport in porous media: role of the secondary energy minimum. *Environ. Sci. Technol.* 38, 1777–1785. doi: 10.1021/es034887l

Ryan, J. N., and Elimelech, M. (1996). Colloid mobilization and transport in groundwater. *Colloid. Surf. A Physicochem. Eng. Aspects* 107, 1–56. doi: 10.1016/0927-7757(95)03384-X

Sadeghi, G., Schijven, J. F., Behrends, T., Hassanizadeh, S. M., Gerritse, J., and Kleingeld, P. J. (2011). Systematic study of effects of pH and ionic strength on attachment of phage PRD1. *Ground Water* 49, 12–19. doi: 10.1111/j.1745-6584.2010.00767.x

Sasidharan, S., Bradford, S. A., Šimunek, J., Torkzaban, S., and Vanderzalm, J. (2017a). Transport and fate of viruses in sediment and stormwater from a managed aquifer recharge site. *J. Hydrol.* 555, 724–735. doi: 10.1016/j.jhydrol.2017.10.062

Sasidharan, S., Torkzaban, S., Bradford, S. A., Cook, P. G., and Gupta, V. V. S. R. (2017b). Temperature dependency of virus and nanoparticle transport and retention in saturated porous media. *J. Contaminant Hydrol.* 196, 10–20. doi: 10.1016/j.jconhyd.2016.11.004

Schijven, J. F., Hassanizadeh, S. M., Dowd, S. E., and Pillai, S. D. (2000). Modeling virus adsorption in batch and column experiments. *Quantitat. Microbiol.* 2, 5–20. doi: 10.1023/A:1010062728286

Schijven, J. F., Sadeghi, G., and Hassanizadeh, S. M. (2016). Long-term inactivation of bacteriophage PRD1 as a function of temperature, pH, sodium and calcium concentration. *Water Res.* 103, 66–73. doi: 10.1016/j.watres.2016.07.010

Schinner, T., Letzner, A., Liedtke, S., Castro, F. D., Eydelnant, I. A., and Tufenkji, N. (2010). Transport of selected bacterial pathogens in agricultural soil and quartz sand. *Water Res.* 44, 1182–1192. doi: 10.1016/j.watres.2008.11.038

Seetha, N., Kumar, M. M., and Hassanizadeh, S. M. (2015b). Modeling the co-transport of viruses and colloids in unsaturated porous media. *J. Contaminant Hydrol.* 181, 82–101. doi: 10.1016/j.jconhyd.2015.01.002

Seetha, N., Majid Hassanizadeh, S., Mohan Kumar, M. S., and Raoof, A. (2015a). Correlation equations for average deposition rate coefficients of nanoparticles in a cylindrical pore. *Water Resour. Res.* 51, 8034–8059, doi: 10.1002/2015WR017723

Seetha, N., Raoof, A., Mohan Kumar, M. S., and Majid Hassanizadeh, S. (2017). Upscaling of nanoparticle transport in porous media under unfavorable conditions: pore scale to Darcy scale. *J. Contaminant Hydrol.* 200, 1–14. doi: 10.1016/j.jconhyd.2017.03.002

Shen, C., Huang, Y., Li, B., and Jin, Y. (2008). Effects of solution chemistry on straining of colloids in porous media under unfavorable conditions. *Water Resour. Res.* 44, 1–12. doi: 10.1029/2007WR006580

Sun, Y., Gao, B., Bradford, S. A., Wu, L., Chen, H., Shi, X., et al. (2015). Transport, retention, and size perturbation of graphene oxide in saturated porous media: effects of input concentration and grain size. *Water Res.* 68, 24–33. doi: 10.1016/j.watres.2014.09.025

Syngouna, V. I., and Chrysikopoulos, C. V. (2012). Transport of biocolloids in water saturated columns packed with sand: effect of grain size and pore water velocity. *J. Contaminant Hydrol*, 129–130, 11–24. doi: 10.1016/j.jconhyd.2012.01.010

Syngouna, V. I., and Chrysikopoulos, C. V. (2013). Cotransport of clay colloids and viruses in water saturated porous media. *Colloids Surf. A.* 416, 56–65, doi: 10.1016/j.colsurfa.2012.10.018

Syngouna, V. I., and Chrysikopoulos, C. V. (2015). Experimental investigation of virus and clay particles cotransport in partially saturated columns packed with glass beads. *J. Colloid Interface Sci.* 440, 140–150. doi: 10.1016/j.jcis.2014.10.066

Tian, Y., Gao, B., Silvera-Batista, C., and Ziegler, K. J. (2010). Transport of engineered nanoparticles in saturated porous media. *J. Nanoparticle Res.* 12, 2371–2380. doi: 10.1007/s11051-010-9912-7

Toloni, I., Lehmann, F., and Ackerer, P. (2014). Modeling the effects of water velocity on TiO_2 nanoparticles transport in saturated porous media. *J. Contaminant Hydrol.* 171, 42–48. doi: 10.1016/j.jconhyd.2014.10.004

Tong, M., and Johnson, W. P. (2006). Excess colloid retention in porous media as a function of colloid size, fluid velocity, and grain angularity. *Environ. Sci. Technol.* 40, 7725–7731. doi: 10.1021/es061201r

Tong, M., Li, X., Brow, C. N., and Johnson, W. P. (2005). Detachment-influenced transport of an adhesion-deficient bacterial strain within water-reactive porous media. *Environ. Sci. Technol.* 39, 2500–2508. doi: 10.1021/es049013t

Torkzaban, S., Bradford, S. A., van Genuchten, M. T., and Walker, S. L. (2008a). Colloid transport in unsaturated porous media: the role of water content and ionic strength on particle straining. *J. Contaminant Hydrol.* 96, 113–127. doi: 10.1016/j.jconhyd.2007.10.006

Torkzaban, S., Tazehkand, S. S., Walker, S. L., and Bradford, S. A. (2008b). Transport and fate of bacteria in porous media: coupled effects of chemical conditions and pore space geometry. *Water Resour. Res.* 44:6541. doi: 10.1029/2007WR006541

Tufenkji, N., and Elimelech, M. (2004). Correlation equation for predicting single-collector efficiency in physicochemical filtration in saturated porous media. *Environ. Sci. Technol.* 38, 529–536. doi: 10.1021/es034049r

Tufenkji, N., and Elimelech, M. (2005). Breakdown of colloid filtration theory: role of the secondary energy minimum and surface charge heterogeneities. *Langmuir* 21, 841–852. doi: 10.1021/la048102g

Wan, J., and Tokunaga, T. K. (2002). Partitioning of clay colloids at air–water interfaces. *J. Colloid Interface Sci.* 247, 54–61. doi: 10.1006/jcis.2001.8132

Wang, C., Bobba, A. D., Attinti, R., Shen, C., Lazouskaya, V., Wang, L. P., et al. (2012). Retention and transport of silica nanoparticles in saturated porous media: effect of concentration and particle size. *Environ. Sci. Technol.* 46, 7151–7158. doi: 10.1021/es300314n

Wang, M., Gao, B., Tang, D., Sun, H., Yin, X., and Yu, C. (2017). Effects of temperature on graphene oxide deposition and transport in saturated

porous media. *J. Hazard. Mater*. 331, 28–35. doi: 10.1016/j.jhazmat.2017.02.014

Yao, K.-M., Habibian, M. T., and O'Melia, C. R. (1971). Water and waste water filtration: concepts and applications. *Environ. Sci. Technol*. 5, 8153–8158. doi: 10.1021/es60058a005

Zhang, L., Hou, L., Wang, L., Kan, A. T., Chen, W., and Tomson, M. B. (2012). Transport of fullerene nanoparticles (nC60) in saturated sand and sandy soil: controlling factors and modeling. *Environ. Sci. Technol*. 46, 7230–7238. doi: 10.1021/es301234m

Conflict of Interest: The authors declare that the research was conducted in the absence of any commercial or financial relationships that could be construed as a potential conflict of interest.

Publisher's Note: All claims expressed in this article are solely those of the authors and do not necessarily represent those of their affiliated organizations, or those of the publisher, the editors and the reviewers. Any product that may be evaluated in this article, or claim that may be made by its manufacturer, is not guaranteed or endorsed by the publisher.